Supporting Information

Enhancing Li-O_2 battery performance with conductive hierarchical metal-organic framework composite cathodes

Pingan Pan[a], Si Miao[a], Ying Zhang[a], Shilin Huo[a], Doufeng Wu[a,*], and Sanchuan Yu[a,*]

[a] School of Chemistry and Chemical Engineering, Zhejiang Sci-Tech University, Hangzhou 310018, People's Republic of China

* Corresponding author: Zhejiang Sci-Tech University, School of Chemistry and Chemical Engineering, Hangzhou 310018, People's Republic of China.

Tel.: +86-571-86843217; Fax: +86-571-86843217.

E-mail: dfwu@zstu.edu.cn (D. Wu), yuschn@163.com (S. Yu),

1. Experimental section

1.1 Preparation of G-OH, $M_3(HHTP)_2$, $M_xM_{3-x}(HHTP)_2$ and their composites

G-OH: The preparation of G-OH follows the method described in a previous work [1]. 100 mL of graphene dispersion with a concentration of 1 mg mL^{-1} and 0.98 g ferrous chloride was added to a flask, 0.1 mol L^{-1} dilute HCl solution was used to adjust the pH acidity to 4. Then, heated to 35 ℃ and stirred for 2 h, with H_2O_2 and deionized water were diluted at a volume ratio of 1:3 and subsequently added to the reaction system using a micro-injection pump at an injection rate of 50 mL h^{-1}. The reaction product was filtered and washed with 0.1 mol L^{-1} HCl to remove residual ions, and potassium thiocyanate was used to check whether the iron ions were removed. The product was then washed with deionized water until neutral. Finally, the product was dispersed in water for later use.

$Cu_3(HHTP)_2$: 0.3mmol $Cu(CH_3COO)_2 \cdot H_2O$, 0.2 mmol 2, 3, 6, 7, 10, 11-hexahydroxytriphenylene (HHTP), 15 mL of deionized water in a 20 mL glass bottle and sonicated for 30 minutes until the solid dissolved. The bottle was then vigorously swirled and shortly sonicated resulting in a dark solution. The reaction mixture was heated in an isothermal oven at 85 °C for 24 h resulting in dark blue crystals and cooled naturally to room temperature. Finally, the crystals were washed first with deionized water (3×15mL), and then with acetone (6×15mL). After centrifugation, placed it in a vacuum drying box and heated at 80 °C for 12h. The preparation method of $Ni_3(HHTP)_2$ is the same as $Cu_3(HHTP)_2$ except replacing $Cu(CH_3COO)_2 \cdot H_2O$ with $Ni(CH_3COO)_2 \cdot 4H_2O$.

$Cu_{1.5}Ni_{1.5}(HHTP)_2$: The preparation method is consistent with $Cu_3(HHTP)_2$, and the molar ratio between the bimetallic salts is 1:1. 0.15mmol $Cu(CH_3COO)_2·H_2O$, 0.15mmol $Ni(CH_3COO)_2·4H_2O$, 0.2mmol 2, 3, 6, 7, 10, 11-hexahydroxytriphenylene (HHTP), 15 mL of deionized water in a 20 mL glass bottle and sonicated for 30 minutes until the solid dissolved. The reaction mixture was heated in an isothermal oven at 85 °C for 24 h and cooled naturally to room temperature. Finally, the crystals were washed first with deionized water (3×15mL), and then with acetone (6×15mL). After centrifugation, placed it in a vacuum drying box and heated at 80 °C for 12h.

monometallic composites $[Cu_3(HHTP)_2]_x$-$(G\text{-}OH)_y$: After ultrasonically treating the G-OH aqueous dispersion for 1 h, $Cu(CH_3COO)_2·H_2O$ and G-OH were added to the mixture at mass ratios of 3:1, 1:1, and 1:3, respectively. Added 20 mL deionized water in a 100 mL glass bottle, and ultrasonically dispersed uniformly, and stirred for 1 h at room temperature to form solution A. HHTP (molar ratio to $Cu(CH_3COO)_2·H_2O$ is 2:3) was putted into a 20 mL bottle, added 10 mL of deionized water, ultrasonically dispersed it evenly, poured it into solution A, continued to stir until it was evenly mixed, and heated in an isothermal oven at 85 °C for 24 h. The reaction mixture was naturally cooled to room temperature, and the crystals were washed with deionized water (3×15mL), followed by acetone (6×15mL). After centrifugation, placed it in a vacuum drying box and heated at 80 °C for 12h to obtain $[Cu_3(HHTP)_2]_1$-$(G\text{-}OH)_1$, $[Cu_3(HHTP)_2]_1$-$(G\text{-}OH)_3$, and $[Cu_3(HHTP)_2]_3$-$(G\text{-}OH)_1$. The preparation method of $[Ni_3(HHTP)_2]_x$-$(G\text{-}OH)_y$ is the same as $[Cu_3(HHTP)_2]_x$-$(G\text{-}OH)_y$.

bimetallic composites $[Cu_{1.5}Ni_{1.5}(HHTP)_2]_x$-$(G\text{-}OH)_y$: The preparation method is consistent with $[Cu_3(HHTP)_2]_x$-$(G\text{-}OH)_y$, bimetallic salts and G-OH were added to the mixture at mass ratios of 3:1, 1:1, and 1:3, respectively. The molar ratio between the bimetallic salts is 1:1. Added 20 mL deionized water in a 100 mL glass bottle, and ultrasonically dispersed uniformly, and stirred for 1 h at room temperature to form solution A. HHTP (molar ratio to bimetallic salts is 2:3) was putted into a 20 mL bottle, added 10 mL of deionized water, ultrasonically dispersed it evenly, poured it into solution A, continued to stir until it was evenly mixed, and heated in an isothermal oven at 85 °C for 24 h. The reaction mixture was naturally cooled to room temperature, and the crystals were washed with deionized water (3×15mL), followed by acetone (6×15mL). After centrifugation, placed it in a vacuum drying box and heated at 80 °C for 12h to obtain $[Cu_{1.5}Ni_{1.5}(HHTP)_2]_1$-$(G\text{-}OH)_1$, $[Cu_{1.5}Ni_{1.5}(HHTP)_2]_1$-$(G\text{-}OH)_3$, and $[Cu_{1.5}Ni_{1.5}(HHTP)_2]_3$-$(G\text{-}OH)_1$.

1.2 Materials characterization

Its morphology and element distribution were characterized by scanning electron microscopy (SEM, Hitachi SU8100). The crystal phase of powders and electrodes was examined by X-ray diffraction (XRD, Bruker AXS GmbH, Copper Kα, λ=1.54178 Å) in the 2θ range of 2.0-60.0° at the scan rate of 2.4° min^{-1} in steps of 0.02°. Elemental content analysis of materials was measured by inductively coupled plasma optical emission spectrometry (ICP-OES) after appropriate dilution. Nitrogen adsorption and desorption method (Micrometrics Corporation, ASAP 3020, 77K) was

used to obtain the specific surface area and pore size distribution of the samples by BET and BJH methods, respectively. The AC electrochemical impedance of the battery was determined by the electrochemical workstation (CHI604E).

1.3 Preparation of cathode material

The cathodes were prepared by casting a slurry of the material on a hydrophobic carbon paper. The slurry consisted of 80 wt% synthesized materials as the catalyst and 20 wt% polyvinylidene fluoride dispersed in 1-methyl-2-pyrrolidone, and the catalyst loading was maintained at approximately 2-3 mg. After casting, the cathodes were dried in a vacuum oven at 80 °C for 24 h.

When assembled into lithium-oxygen batteries, the amount of active material was recalculated based on the size difference between the battery mold diameter (10 mm) and the carbon paper substrate diameter (16 mm), using the following equation:

Amount of active material = catalyst loading × (5^2) / (8^2).

1.4 Electrochemical measurements

The battery was assembled in a glove box filled with pure argon. Li / separator (Celgard 2400) (dipped with electrolyte) / O_2 electrode was sealed into a Swagelok cell with an air hole placed on the positive electrode side to allow the oxygen to flow in. A Swagelok cell was assembled with three layer separator (Celgard 2400), a lithium foil anode (thickness, 500 μm), and 400 μl of 1.0 M bis(trifluoromethane) sulfonamide lithium salt (LiTFSI) in tetraethylene glycol dimethyl ether electrolyte.

After assembly, the batteries were stabilized in a pure oxygen atmosphere for 6 h at room temperature. All the cell performance evaluations were based on the weight of synthesized materials with a total loading of 0.7-1.2 mg. The full charge-discharge profiles of Li-O_2 cells were tested in the voltage window from 2.0 to 4.5 V and at a rate of 500 mA g^{-1} in a LAND cycler (Wuhan Land Electronic Co. Ltd). The cycling test was conducted at a specific capacity limit of 500 mAh g^{-1} at a current density of 50 mA g^{-1}. Electrochemical impedance spectroscopy (EIS) was measured at an AC voltage of 5 mV amplitude in the frequency range between 0.01 Hz and 10^5 Hz.

2. Results and discussion

2.1 Catalyst characterizations

The peaks for $Cu_{1.5}Ni_{1.5}(HHTP)_2$ are consistent with those of monometallic composites shown in Fig. S1, suggesting similar structural characteristics.

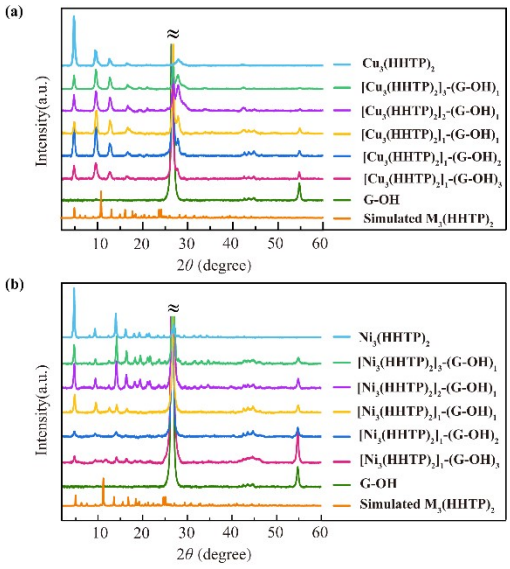

Fig. S1. XRD patterns of $M_3(HHTP)_2$, G-OH and their composites.

(a) $Cu_3(HHTP)_2$. (b) $Ni_3(HHTP)_2$.

From the SEM patterns, it can be seen that the content of G-OH affects the stability and morphology of the composite material: decreasing G-OH content leads to the formation of spherical $Cu_{1.5}Ni_{1.5}(HHTP)_2$ aggregates due to the diminished stability (Fig. S2), whereas increasing G-OH leads to smaller and slightly incomplete crystal structures, resulting in a rough and wrinkled appearance on the surface (Fig. S3).

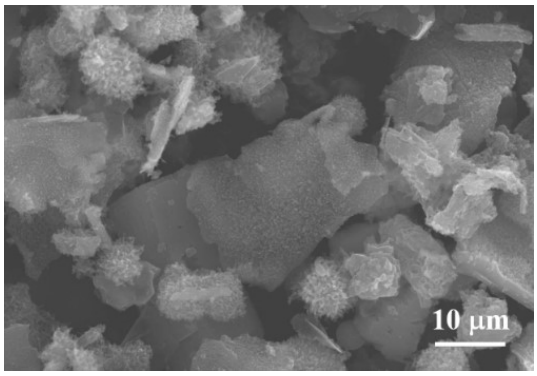

Fig. S2. SEM pattern of $[Cu_{1.5}Ni_{1.5}(HHTP)_2]_3$-$(G\text{-}OH)_1$.

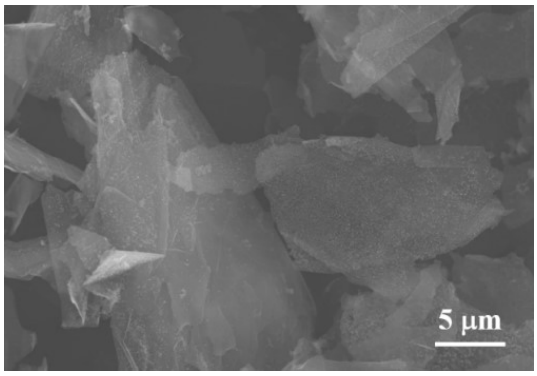

Fig. S3. SEM pattern of $[Cu_{1.5}Ni_{1.5}(HHTP)_2]_1$-$(G\text{-}OH)_3$.

The presence of Cu, Ni, C, and O elements were confirmed in Fig. S4.

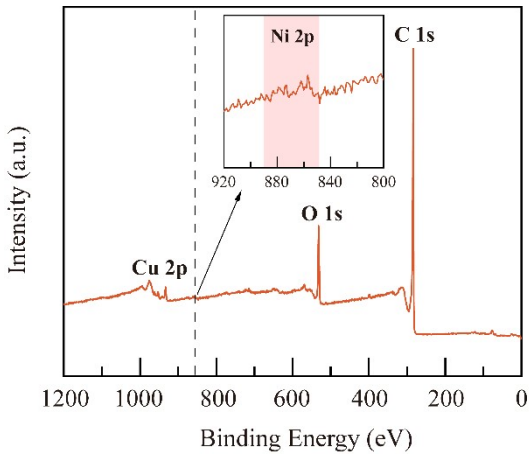

Fig. S4. XPS survey spectra of $[Cu_{1.5}Ni_{1.5}(HHTP)_2]_1$-$(G\text{-}OH)_1$.

2.2 Electrochemical performance of Li-O_2 batteries

Fig. S5 illustrates that the electrochemical performance of bimetallic composite material $[Cu_{1.5}Ni_{1.5}(HHTP)_2]_1$-$(G\text{-}OH)_1$ (12542 mAh g^{-1}, 1.5V) surpasses that of bimetallic $Cu_{1.5}Ni_{1.5}(HHTP)_2$ (4107 mAh g^{-1}, 1.85V), monometallic $Cu_3(HHTP)_2$ (1695 mAh g^{-1}, 2.05V) and $Ni_3(HHTP)_2$ (1428 mAh g^{-1}, 2.1V), and monometallic composite materials $[Cu_3(HHTP)_2]_1$-$(G\text{-}OH)_1$ (5707 mAh g^{-1}, 1.8 V) and $[Ni_3(HHTP)_2]_1$-$(G\text{-}OH)_1$ (6200 mAh g^{-1}, 1.7 V) versions.

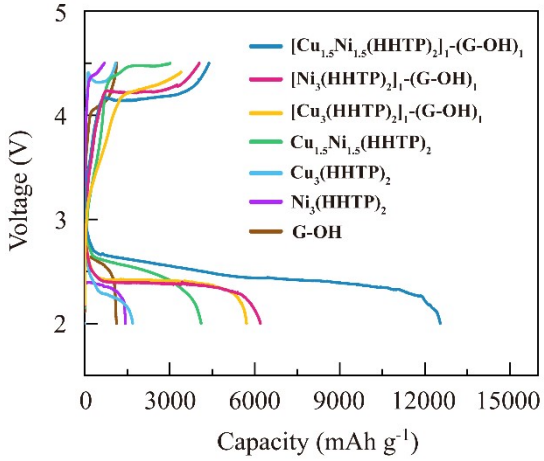

Fig. S5. Galvanostatic discharge−charge curves of Li-O_2 batteries with different oxygen cathodes measured at a current density of 50 mAh g^{-1}.

At current densities of 50, 100, and 200 mA g^{-1}, the specific capacity of the $[Cu_{1.5}Ni_{1.5}(HHTP)_2]_1$-$(G\text{-}OH)_1$ cathode is recorded at 12542, 6338, and 4289 mAh g^{-1}, respectively. In comparison, under identical conditions, bimetallic composite outperforms the monometallic composite materials $[Cu_3(HHTP)_2]_1$-$(G\text{-}OH)_1$ (6536, 4744, and 2930 mAh g^{-1}) (Fig. S6) and $[Ni_3(HHTP)_2]_1$-$(G\text{-}OH)_1$ (6200, 4804, and 2723 mAh g^{-1}) (Fig. S7).

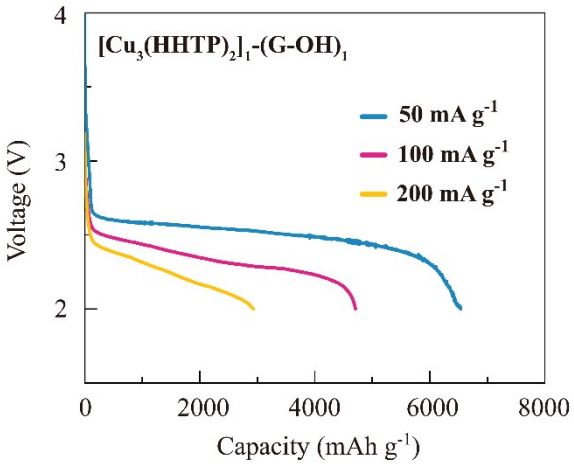

Fig. S6. $[Cu_3(HHTP)_2]_1$-$(G\text{-}OH)_1$ rate performances of Li-O_2 batteries.

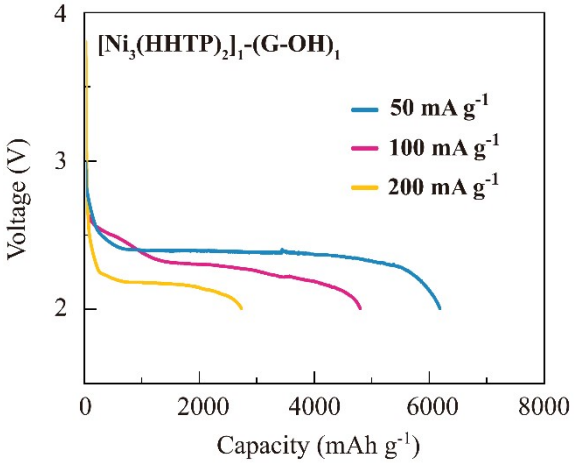

Fig. S7. $[Ni_3(HHTP)_2]_1$-$(G\text{-}OH)_1$ rate performances of Li-O_2 batteries.

The batteries with the $[Cu_{1.5}Ni_{1.5}(HHTP)_2]_1$-$(G\text{-}OH)_1$ cathode achieved 40 cycles with a discharge terminal voltage maintained above 2 V and exhibited an initial charge-discharge overpotential of 1.1 V. For comparison, $[Cu_3(HHTP)_2]_1$-$(G\text{-}OH)_1$ achieved only 20 cycles with overpotentials between 2.5-2.7 V (Fig. S8), and $[Ni_3(HHTP)_2]_1$-$(G\text{-}OH)_1$ lasted for 29 cycles with overpotentials between 2.4-2.7 V (Fig. S9).

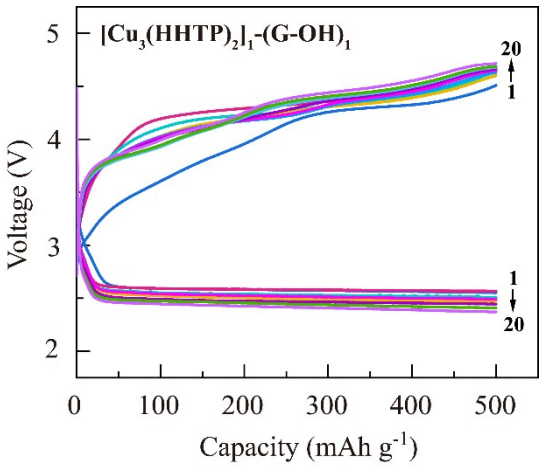

Fig. S8. $[Cu_3(HHTP)_2]_1$-$(G\text{-}OH)_1$ cycle performance under a specific capacity limit of 500 mAh g^{-1} at a current density of 50 mA g^{-1}.

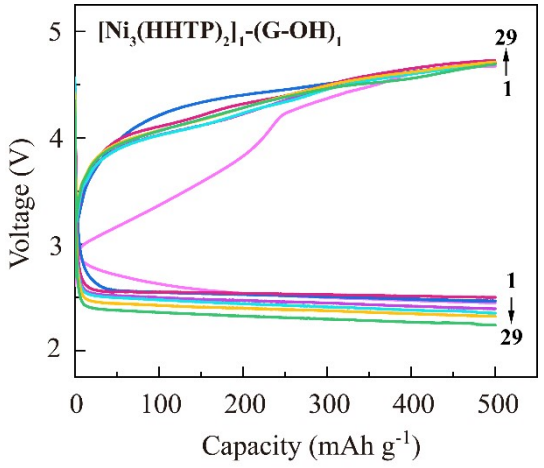

Fig. S9. $[Ni_3(HHTP)_2]_1$-$(G\text{-}OH)_1$ cycle performance under a specific capacity limit of 500 mAh g^{-1} at a current density of 50 mA g^{-1}.

The EIS results reveal a lower impedance of 52.8Ω for $[Cu_{1.5}Ni_{1.5}(HHTP)_2]_1$-(G-OH)$_1$ compared to monometallic composite materials $[Cu_3(HHTP)_2]_1$-(G-OH)$_1$ (65.8Ω) and $[Ni_3(HHTP)_2]_1$-(G-OH)$_1$ (69.11Ω), as shown in Fig. S10.

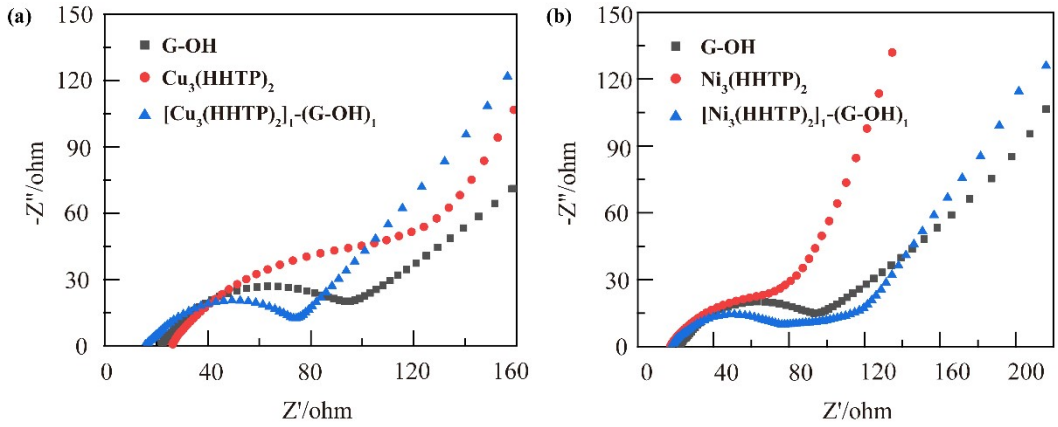

Fig. S10. EIS curves of Li-O_2 batteries with different oxygen cathodes.

(a) $[Cu_3(HHTP)_2]_1$-(G-OH)$_1$. (b) $[Ni_3(HHTP)_2]_1$-(G-OH)$_1$.

The mass compositions of the components within the composite material were quantified using inductively coupled plasma-optical emission spectrometer (ICP-OES), with findings presented in Table S1.

Table S1 ICP results (The mass fractions of each component in the composites).

Sample Name	M	Cu	Ni	$M_3(HHTP)_2$	G-OH
$[Cu_{1.5}Ni_{1.5}(HHTP)_2]_1$-(G-OH)$_1$	23.60	1.392 (5.9%)	0.4484 (1.9%)	8.229	15.37
$Cu_{1.5}Ni_{1.5}(HHTP)_2$	26.10	2.871 (11.0%)	0.914 (3.5%)	16.92	-

Table S2 compares the specific discharge capacity and cycling performance of the Li-O_2 battery cathode materials from this study with previously reported materials. Notably, the specific discharge capacity of $[Cu_{1.5}Ni_{1.5}(HHTP)_2]_1$-$(G\text{-}OH)_1$ synthesized in this study reaches an impressive 12542 mAh g^{-1} at a current density of 50 mA g^{-1}, surpassing several previously reported cathode materials.

Table S2. Performance comparison of Li-O_2 batteries with different oxygen electrodes.

Catalysts	Capacity (mAh g^{-1})	Cycle number	Ref.
$[Cu_{1.5}Ni_{1.5}(HHTP)_2]_1$-$(G\text{-}OH)_1$	12542 mAh g^{-1} at 50 mA g^{-1}	40 cycles at 50 mA g^{-1} and 500 mAh g^{-1}	This work
Tz-Mg-MOF-74	7700 mAh g^{-1} at 50 mA g^{-1}	28 cycles at 200 mA g^{-1} and 600 mAh g^{-1}	[2]
Co@N/S-CNF	9290.7 mAh g^{-1} at 50 mA g^{-1}	42 cycles at 100 mA g^{-1} and 500 mAh g^{-1}	[3]
Dy-BTC	7618 mAh g^{-1} at 50 mA g^{-1}	76 cycles at 200 mA g^{-1} and 1000 mAh g^{-1}	[4]
ZrO_2@$NiCo_2O_4$/GNS	9034 mAh g^{-1} at 50 mA g^{-1}	100 cycles at 100 mA g^{-1} and 1000 mAh g^{-1}	[5]
Ni-MOFs	9000 mAh g^{-1} at 0.12 mA cm^{-1}	170 cycles at 0.6 mA cm^{-1} and 600 mAh g^{-1}	[6]
2D Mn-MOF	9464 mAh g^{-1} at 100 mA g^{-1}	200 cycles at 100 mA g^{-1} and 1000 mAh g^{-1}	[7]
Co-MOF-74	11350 mAh g^{-1} at 100 mA g^{-1}	8 cycles at 250 mA g^{-1} and 1000 mAh g^{-1}	[8]
MnCo-MOF-74	11150 mAh g^{-1} at 200 mA g^{-1}	44 cycles at 200 mA g^{-1} and 1000 mAh g^{-1}	[9]

CoP@PNCF-700	9630.5 mAh g^{-1} at 100 mA g^{-1}	187 cycles at 200 mA g^{-1} and 500 mAh g^{-1}	[10]
Co_3O_4/CT	6509 mAh g^{-1} at 200 mA g^{-1}	134 cycles at 200 mA g^{-1} and 1000 mAh g^{-1}	[11]
Co_3O_4@ $NiCo_2O_4$	11672.8 mAh g^{-1}	280 cycles	[12]
RuO_2/Co-N-C	16671 mAh g^{-1} at 200 mA g^{-1}	174 cycles at 200 mA g^{-1} and 500 mAh g^{-1}	[13]
Ru/Co@CoN_x-C	17050 mAh g^{-1} at 300 mA g^{-1}	205 cycles at 300 mA g^{-1} and 1000 mAh g^{-1}	[14]

References

[1] H. Deng, J. Huang, C. Qin, T. Xu, H. Ni, P. Ye, Preparation of high-performance nanocomposite membranes with hydroxylated graphene and graphene oxide. Journal of Water Process Engineering, 2021, 40, 101945.

[2] N. Li, Z. Chang, M. Zhong, Z. Fu, J. Luo, Y. Zhao, Functionalizing MOF with Redox-Active Tetrazine Moiety for Improving the Performance as Cathode of Li-O_2 Batteries, CCS Chemistry, 2021, 3(3), 1297-1305.

[3] S. Guo, Y. Sun, J. Wang, L. Peng, H. Li, C. Li, Bimetallic ZIF-derived cobalt nanoparticles anchored on N- and S-codoped porous carbon nanofibers as cathode catalyst for Li-O_2 batteries, Electrochimica Acta, 2022, 418.

[4] D. Liu, X. Zhang, Y. Wang, S. Song, L. Cui, H. Fan, A new perspective of lanthanide metal-organic frameworks: tailoring Dy-BTC nanospheres for rechargeable Li-O_2 batteries, Nanoscale, 2020, 12(17), 9524-9532.

[5] R. Palani, Y. Wu, S. Wu, R. Jose, C. Yang, Metal-organic framework-derived ZrO_2/$NiCo_2O_4$/graphene mesoporous cake-like structure as enhanced bifunctional electrocatalytic cathodes for long life Li-O_2 batteries, Electrochimica Acta, 2022, 412.

[6] X. Hu, Z. Zhu, F. Cheng, Z. Tao, J. Chen, Micro-nano structured Ni-MOFs as high-performance cathode catalyst for rechargeable Li-O_2 batteries, Nanoscale, 2015, 7(28), 11833-11840.

[7] M. Yuan, R. Wang, W. Fu, L. Lin, Z. Sun, X. Long, Ultrathin Two-Dimensional Metal Organic

Framework Nanosheets with the Inherent Open Active Sites as Electrocatalysts in Aprotic Li-O_2 Batteries, Acs Applied Materials & Interfaces, 2019, 11(12), 11403-11413.

[8] W. Yan, Z. Guo, H. Xu, Y. Lou, J. Chen, Q. Li, Downsizing metal–organic frameworks with distinct morphologies as cathode materials for high-capacity Li–O_2 batteries, Materials Chemistry Frontiers, 2017, 1, 1324-1330.

[9] S.H. Kim, Y.J. Lee, D.H. Kim, Y.J. Lee, Bimetallic metal–organic frameworks as efficient cathode catalysts for Li–O_2 batteries, ACS Applied Materials & Interfaces, 2018, 10, 660-667.

[10] L. Zhang, S. Luo, P. Li, M. Sun, S. Yan, MOF-derived CoP nanoparticles anchored on P, N co-doped carbon nanoframework as robust electrocatalyst for rechargeable Li-O_2 batteries, Journal of Energy Storage, 2023, 74.

[11] H. Gong, T. Wang, H. Xue, X. Lu, W. Xia, L. Song, Spatially-controlled porous nanoflake arrays derived from MOFs: An efficiently long-life oxygen electrode, Nano Research, 2019, 12(10), 2528-2534.

[12] Y. Zhao, L. Ding, X. Wang, X. Yang, J. He, B. Yang, Yolk-shell ZIF-8@ZIF-67 derived Co_3O_4@$NiCo_2O_4$ catalysts with effective electrochemical properties for Li-O_2 batteries, Journal of Alloys and Compounds, 2021, 861.

[13] Y. Zhu, T. Zhang, Q. Li, Z. Xue, M. Yu, J. Li, MOFs-derived 3D nanoporous Co-N-C coupled with RuO_2 composite as enhanced catalysts for Li-O_2 batteries, Journal of Alloys and Compounds, 2024, 983.

[14] Z. Tong, C. Lv, Y. Zhou, P. Zhang, C. Xiang, Z. Li, Highly Dispersed Ru-Co Nanoparticles Interfaced With Nitrogen-Doped Carbon Polyhedron for High Efficiency Reversible Li-O_2 Battery, Small, 2022, 18(48).